Very High Cycle Fatigue Behaviour of the 316L Weldment Fabricated By Laser Butt-Welding

Very High Cycle Fatigue Behaviour of the 316L Weldment Fabricated By Laser Butt-Welding

Z H Xiong[1], X F Ma[1,*], X Y Qi[2]

[1]Sino-French Institute of Nuclear Engineering and Technology, Sun Yat-sen University, Zhuhai 519082, China
[2]Wuhan Huagong Laser Engineering Co., Ltd., Wuhan 430074, China

[*]Corresponding author: maxf6@mail.sysu.edu.cn

Abstract. In nuclear industry, 316L weldments are widely used in components fabricating, which usually suffer from very-high-cycle fatigue. Therefore, the very high cycle fatigue (VHCF) behaviour of 316L weldment fabricated by laser butt-welding joint were studied using an ultrasonic fatigue testing system. The microscopic examination indicated that an evident pore is observed in the weld seam and the fine columnar-dendrite structure is formed in the central part of the weld seam. Near the weld interface in the weld seam, the weld microstructure shows larger columnar-dendrite. The hardness distribution of the weldment is to coincide with the characteristic of the microstructure. In the central part of the weld seam, the hardness is the highest, and is the lowest in the base metal. Fatigue failure still occurred in the VHCF regime. The fatigue crack initiated from the internal pores caused by laser butt-welding. Although the fatigue strength of weld seam might be decreased due to the pore, the fatigue strength of the weldment was the same as the base metal in this research. That is, the defect with a certain size in the weld seam does not affect the strength of the weldment.

1. Introduction

316L is widely used as the structural material of nuclear components owing to its excellent corrosive resistance and mechanical properties [1,2]. These components usually suffer from VHCF loading during its service life [3]. Since some researchers [4] found that fatigue failure occurred in the very high cycle regime, more and more researchers started to investigate the very high-cycle fatigue behaviour of steels and alloys [5-7]. It was found that the fatigue crack usually initiated from the internal defect in the VHCF regime and a so-called fish-eye can be observed on the fracture surface, which is different from that of in the low and high-cycle regime. However, the VHCF data of the austenitic stainless steel used as the structural materials of nuclear components is still insufficient [8]. For austenitic stainless steel, the fish-eye is difficult to be observed on the fracture surface [9]. Most of the 316NG specimens failed due to the surface crack initiation, only a specimen failed due to internal crack initial caused by the internal inclusion [8]. The previously research results of the author [3,10] also showed that the fatigue crack initiated from the 316L specimen surface in the VHCF regime. Weld fatigue is a very important design consideration for the application of laser welded component in nuclear industry. However, the fatigue behaviour of 316L weldments in very-high-cycle region has rarely been investigated. The VHCF behaviour of some steel and alloy welds [11,12] indicated that the fatigue crack initiated from subsurface or internal detects caused by welding, and fatigue failure still

occurred in the VHCF regime. The fatigue strength reduced owing to the existence of welding defects and soft zone along the welds. As reported by Hong et al. [7,13,14], fatigue crack usually initiates from internal or subsurface inclusions or defects in the VHCF regime, and the characteristic of the *S-N* curves differs from those of the low- and high-cycle fatigue.
Therefore, in this research, the VHCF behavior of 316L weldments fabricated by laser butt-welding were investigated by an ultrasonic fatigue testing machine. In addition, the microstructure and hardness distribution of the welding seam were investigated. To clarify fatigue crack initiation mechanism, the fatigue fracture surface was investigated through scanning electron microscopy (SEM).

2. Experimental Procedures

2.1. Materials and Specimen Fabrication

Type 316L austenitic stainless steel (or ASTM A240) was used in this research. The yield strength, ultimate tensile strength, and Vickers hardness were 319 MPa, 614 MPa, and 183, respectively. As shown in Figure 1 (a), the 316L welded joint was fabricated by laser butt-welding. The fiber laser head (IPG, YLS-10000) was held by a Robotic arm (KUKA, KR60HA). The laser beam has a circular shape with the diameter of 0.5 mm. The welding parameter used in this study were presented in Table 1. During the welding proceeding, ultra-high purity argon was used as a protecting gas at a flow rate of 25 L/min. The specimens were machined following the geometry shown in Figure 1 (b). Before fatigue testing, each specimen surface was polished using a 1200 grit abrasive paper.

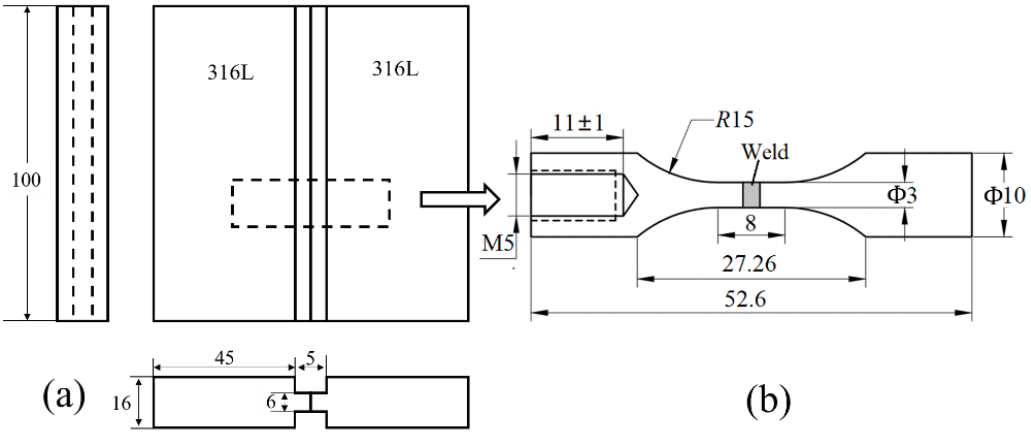

Figure 1. Schematic diagram of specimen fabrication (dimensions: mm) (a) the geometry of the fiber laser welded joint, (b) the size and shape of the ultrasonic fatigue specimen.

Table 1. Laser welding parameter

Laser power (kW)	Welding speed (mm/s)	Beam diameter (mm)	Defocus distance (mm)
6	30	0.5	0

2.2. Measurement of Microstructure and Hardness

The central part of the fatigue specimen with a uniform cross section was cut along the longitudinal direction and mounted in epoxy to study the microstructure and hardness. The samples were ground and polished until a mirror finish was achieved, and were then etched by immersing in an aqueous solution of 15-mL HCl, 5-mL HNO_3, and 100-mL H_2O for approximately 40 min. The specimen microstructures were observed through an optical microscope (VHX-6000). The hardness of the as-received specimens was measured using a Buehler VH1202 indenter under 0.98N before conducting the fatigue test.

2.3. Ultrasonic Fatigue Test

The ultrasonic fatigue tests were performed using an ultrasonic fatigue testing system at 20 kHz with a stress ration of −1 and manually stopped when the fatigue cycles reached up to 10^9. During the fatigue test, loading/arresting interval was applied in addition to the air-cooling of specimen surface to prevent specimen temperature increase. More details information for the ultrasonic fatigue test was reported in literature [15]. After the fatigue test, the fracture surfaces were examined to reveal the fatigue crack initiation and failure mechanism through SEM.

3. Results and Discussions

3.1. Microstructure and Hardness Distribution

The microstructure of the as-received 316L steel is shown in Figure 2(a), where typical austenitic grains are observed. Figure 2 (b) shows the overview image of the weld seam. The weld interface can be observed obviously. An evident pore is observed in the weld seam, which might be caused by the metal evaporation induced by high energy density and protection gas captured by the melted metal. The microstructures of area #1 in the central part of the welding bead is presented in Figure 2(c). The result shows that the fine columnar-dendrite structure is formed in the central part of the weld beam. And the growth directions of such dendrite structure are different, which are distributed symmetrically along the center line. The growth direction is dependent on the heat dissipation path, which is shortest to the base metal. As shown in Figure 2(d), near the weld interface in the weld seam, the weld microstructure shows more columnar-dendrite. This may be due to the fastest heat dissipation in the direction perpendicular to the weld interface. In general, the material properties reduce owing to the grain coarsening in the heat-affected zone. However, in this study, the heat-affected zone was not pronounced, as shown in Figure 2(d), and thus the grains in the base-material area near the welding interface did not grow significantly, which is consistent with the reported results, i.e. the heat-affected zone of 316L weld is not evident [16].

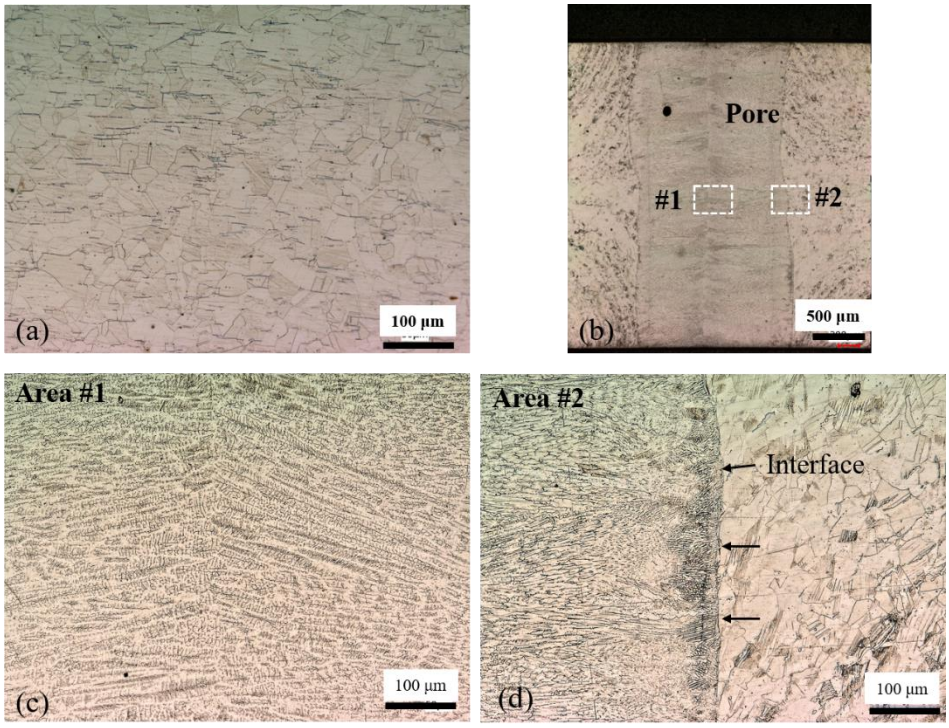

Figure 2. Microstructure of 316L weldment (a) Base metal, (b) Overview of the weld seam, (c) Enlarge view of the area #1 in (b), (d) Enlarge view of the area #2 in (b).

Figure 3 shows the hardness distribution of the weldment. In the central part of the weld seam, the hardness is highest (Hv223 in average) and resulting from the fine columnar-dendrite structure. The hardness of the area near the weld interface in the weld seam is lower than the central part of weld seam but higher than the base metal, which is attributed to the larger columnar-dendrite structure compared to the centre part of the weld seam.

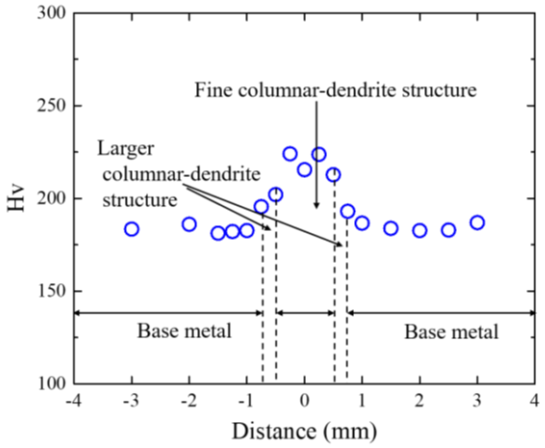

Figure 3. Hardness distribution of the weldment.

3.2. S-N Curve of the Weldment

The relationship between stress amplitude and number of cycles to failure for the 316L weldment is shown in Figure 4. Obviously, the fatigue failure occurred in the very high cycle regime, the plateau region between 10^6-10^7 in convention fatigue was not observed in this research. In the high cycle fatigue regime, most of the specimens failed due to the surface crack initiation, three specimens failed due to subsurface crack initiation. However, in the VHCF regime, most of the specimens failed due to the interior crack initiation except one specimen (surface crack initiation). In other words, the crack tends to initiation from interior of the specimen when the fatigue life beyond 3×10^6 cycles. The similar interior crack initiation behaviour have been observed in other steels and alloys [5,6,13,17]. However, it is different from the results of the investigation on 316L base metal, the fatigue crack initiated from specimen surface in the VHCF regime [3,10].

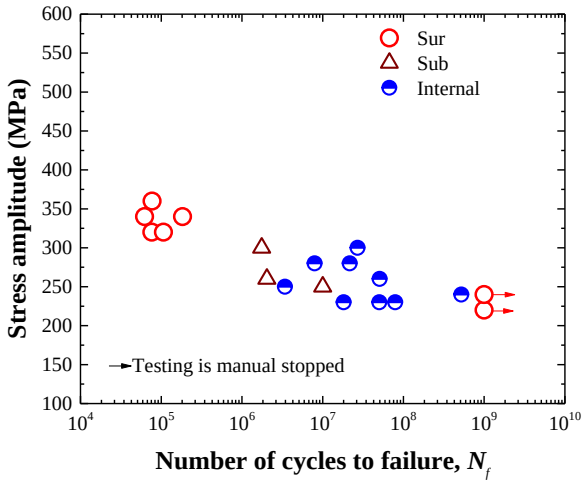

Figure 4. *S-N* curve of the 316L weldment tested at room temperature. Sur: crack initiation from surface, Int: crack initiation from interior, Sub: crack initiation from sub-surface.

Figure 5 shows the comparison between the fatigue strength of 316L weldment and SUS 316L base metal [3]. It should be noted that the fatigue strengths were normalized by its tensile strength in order to eliminate the effect of tensile strength on the fatigue strength. The normalized results showed that the fatigue strength of 316L weldment is almost the same as that of SUS 316L base metal, indicating that the fatigue strength of 316L is not affected by the laser butt-welding process applied in this research, although the pores existed in the weld seam.

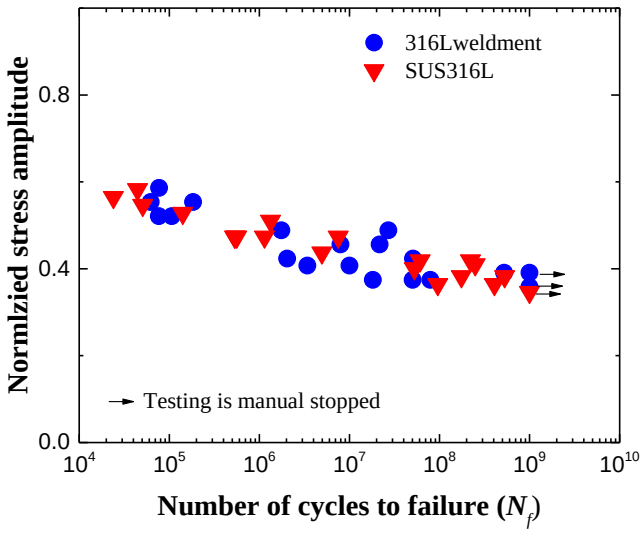

Figure 5. Relationship between normalized stress amplitude and number of cycles to failure

3.3. Fractography

After fatigue tests, the fracture surface of each failed specimen under different stress amplitudes was analyzed through SEM. Most of the specimens were fractured at the weld part. In the low and high cycle fatigue regime, most of the specimens failed due to surface crack initiation. Figure 6 shows the fracture morphology of the specimen tested at 320 MPa and failed at 7.67×10^4 cycles. Obviously, the fatigue crack initiated from the specimen surface and multi-crack initiation sites were observed.

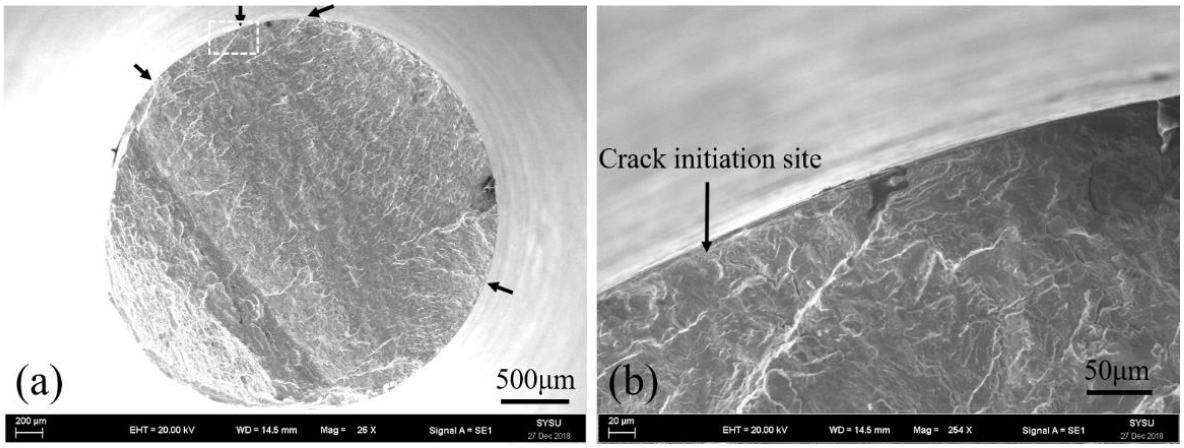

Figure 6. Fracture surface of the specimen tested at 320MPa failed at 7.67×10^4 cycles. (a) Overview of the fracture surface, and (b) Enlargement of the marked rectangle in (a).

Figure 7 shows the fracture surface of the specimen tested at 300MPa failed at 1.75×10^6 cycles. The fatigue crack initiated from the pore caused by the welding at the subsurface. The main crack initiated

at the edge of the large pore, where is adjacent to a smaller pore. In the VHCF regime, all of the specimens failed due to the crack initiation from the pores in the specimen. Figure 8 shows the fracture surface of the specimen tested at 230MPa failed at 7.93×10^7 cycles, i.e. in the VHCF regime. A-so called fish-eye was observed in the crack initiation and propagation area, as shown in the dash cycle in Figure 8 (a). A rough area was located in the fish-eye as shown in Figure 8(b), which was different from the reported results [18], i.e. the rough area was located in the central part of the fish-eye. No inclusion, but a pore was observed in the rough area, which was different from the situation of an inclusion as crack initiation site for steels and alloys [14,15,17]. It was also different from the previously results [3,10], no interior crack initiation was observed for 316L in the very high cycle regime. In general, the crack initiation site of the material, i.e. from surface or interior, is contributed to the competition between the surface defect and interior defect. When the size of the interior defect is large enough, the fatigue crack would initiate from interior. Otherwise, it initiates from surface [19]. Hence, in the case of 316L base metal, due to the good control of inclusion, the fatigue crack initiated from specimen surface. On the contrary, in the case of 316L weldment, due to the existing internal pores, the crack initiated from interior.

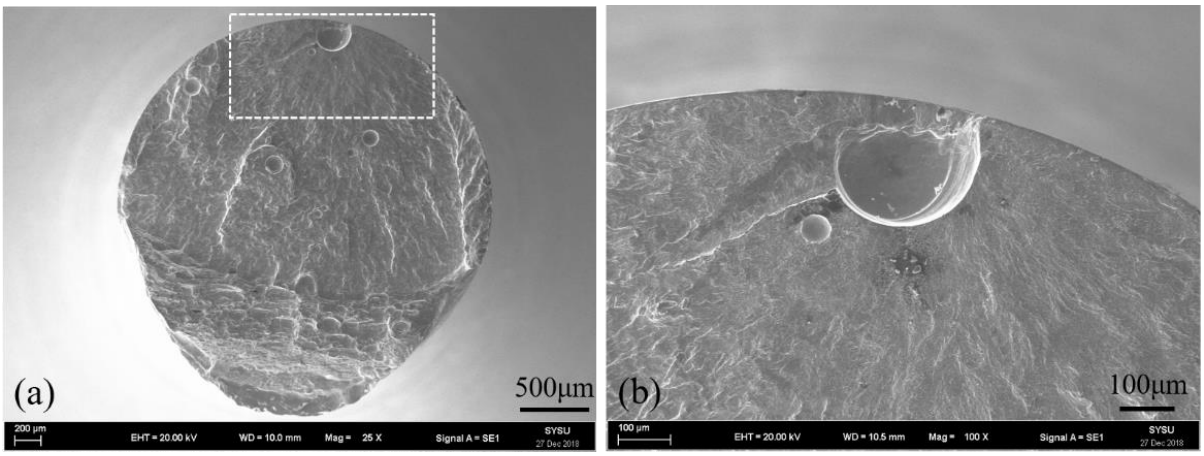

Figure 7. Fracture surface of the specimen tested at 300MPa failed at 1.75×10^6 cycles. (a) Overview of the fracture surface, and (b) Enlargement of the marked rectangle in (a).

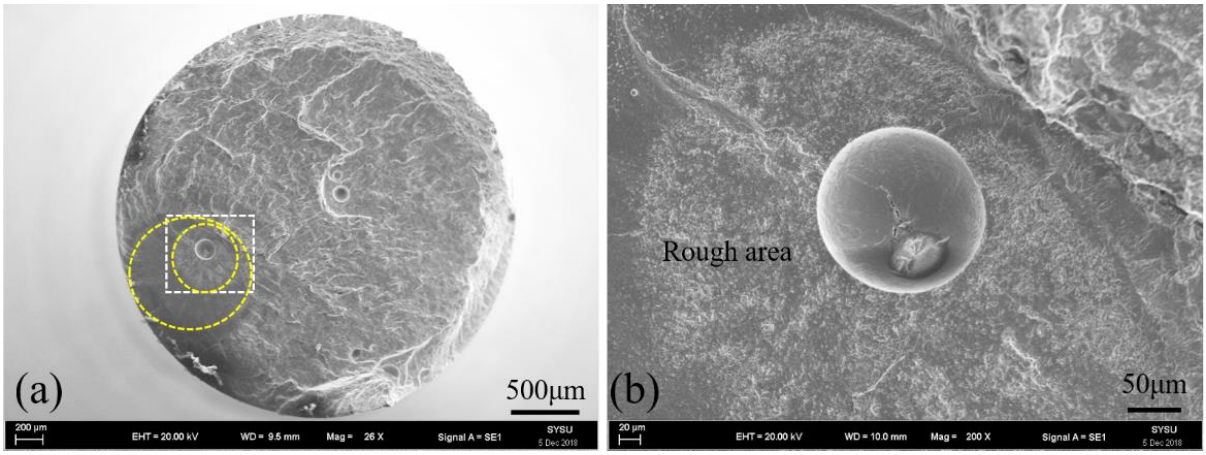

Figure 8. Fracture surface of the specimen tested at 230MPa failed at 7.93×10^7 cycles. (a) Overview of the fracture surface, and (b) Enlargement of the marked rectangle in (a).

4. Conclusions

In this research, the VHCF behaviour of the 316L weldment fabricated by laser butt-welding were investigated by the ultrasonic fatigue testing system. The following conclusions have been drawn:

1) An evident pore is observed in the weld seam, the fine columnar-dendrite structure is formed in the central part of the weld seam and larger columnar-dendrite is observed near the weld interface
2) The hardness distribution is to coincide with the characteristic of the microstructure., the hardness is the highest in the weld seam central and the lowest in the base metal.
3) Fatigue failure still occurred in the VHCF regime. The VHCF crack initiated from the internal pores caused by laser butt-welding. The typical fish-eye was observed at the fracture surface.
4) The fatigue strength of the weldment with pores was the same as the base metal, i.e. the defect with a certain size in the weld seam does not affect the strength of the weldment.

Acknowledgements

This work was financially supported by the Fundamental Research Funds for the Central Universities (Grant No. 17lgpy34), the Natural science foundation of the Guangdong province (Grant 2018A030310102), and the Young Innovative Talent Project of GuangDong Education Department Fund (Gant No. 2016KQNCX004 and 2016KQNCX005). And thanks be to Professor H.Q. Xue and Doctor T. Gao, the ultrasonic fatigue tests were conducted in their lab in Northwestern Polytechnical University.

References

[1] Y. Han, J. Mei, Q. Peng, E. Han, W. Ke, Effect of electropolishing on corrosion of nuclear grade 316L stainless steel in deaerated high temperature water, Corros Sci, 112 (2016) 625-634.
[2] Z. Xiong, T. Naoe, T. Wan, M. Futakawa, K. Maekawa, Mechanical Property Change in the Region of Very High-cycle Fatigue, Procedia Engineering, 101 (2015) 552-560.
[3] T. Naoe, Z. Xiong, M. Futakawa, Gigacycle fatigue behaviour of austenitic stainless steels used for mercury target vessels, J Nucl Mater, 468 (2015) 331-338.
[4] T. Naito, H. Ueda, M. Kikuchi, Observation of fatigue fracture surface of carburized steel, J. Soc. Mater. Sci., Jpn., 32 (1983) 1162-1166.
[5] Z. Ping, G. Gao, R.D.K. Misra, B. Bai, Effect of microstructure on the very high cycle fatigue behavior of a bainite/martensite multiphase steel, Mater Sci Eng A, 630 (2015) 1-7.
[6] S. Siddique, M. Imran, F. Walther, Very high cycle fatigue and fatigue crack propagation behavior of selective laser melted AlSi12 alloy, Int J Fatigue, 94 (2017) 246-254.
[7] Y. Hong, C. Sun, The nature and the mechanism of crack initiation and early growth for very-high-cycle fatigue of metallic materials – An overview, Theoretical & Applied Fracture Mechanics, 92 (2017).
[8] K. Takahashi, T. Ogawa, Evaluation of giga-cycle fatigue properties of austenitic stainless steels using ultrasonic fatigue test, Journal of Solid Mechanics and Materials Engineering, 2 (2008) 366-373.
[9] J. Carstensen, H. Mayer, P. Brøndsted, Very high cycle regime fatigue of thin walled tubes made from austenitic stainless steel, Fatigue Fract Eng M, 25 (2002) 837-844.
[10] T. Naoe, Z. Xiong, M. Futakawa, Temperature measurement for in-situ crack monitoring under high-frequency loading, J Nucl Mater, 506 (2018) 12-18.
[11] W.C. Zhang, M.L. Zhu, K. Wang, F.Z. Xuan, Failure mechanisms and design of dissimilar welds of 9%Cr and CrMoV steels up to very high cycle fatigue regime, Int J Fatigue, (2018).
[12] C. Deng, H. Wang, B. Gong, X. Li, Z. Lei, Effects of microstructural heterogeneity on very high cycle fatigue properties of 7050-T7451 aluminum alloy friction stir butt welds, Int J Fatigue, 83 (2016) 100-108.
[13] Y. Hong, X. Liu, Z. Lei, C. Sun, The formation mechanism of characteristic region at crack

initiation for very-high-cycle fatigue of high-strength steels, Int J Fatigue, 89 (2016) 108-118.
[14] W. Hui, Y. Zhang, X. Zhao, Z. Chao, K. Wang, S. Wei, D. Han, Very high cycle fatigue properties of Cr–Mo low alloy steel containing V-rich MC type carbides, Mater Sci Eng A, 651 (2016) 311-320.
[15] S. Stanzl-Tschegg, Very high cycle fatigue measuring techniques, Int J Fatigue, 60 (2014) 2-17.
[16] S.X. Li, F.Z. Xuan, S.D. Tu, S.S. Yu, Interfacial fatigue crack growth behavior of diffusion bonded joints of 316L stainless steel, Mater Sci Technol, 18 (2010) 141-144.
[17] X. Liu, C. Sun, Y. Hong, Effects of stress ratio on high-cycle and very-high-cycle fatigue behavior of a Ti–6Al–4V alloy, Acta Metallurgica Sinica, 622 (2015) 228-235.
[18] H. Su, X. Liu, C. Sun, Y. Hong, Nanograin layer formation at crack initiation region for very-high-cycle fatigue of a Ti-6Al-4V alloy: Nanograin Formation for VHCF of TI Alloy, Fatigue Fract Eng M, (2017).
[19] L.S. Xin, Very high cycle fatigue properties of high strength steels: effects of nonmetallic inclusions, Metallurgical Industry Press, BeiJing, 2010.